

RESEARCH ARTICLE

10.1002/2014GC005272

Key Points:

- The Society Islands indicate a highstand at ~ 5.4 to ~ 2 ka
- Sea level has dropped by ~ 1.8 m since the Holocene maximum
- For microatolls geoid deformation and subsidence rate should be considered

Correspondence to:

R. Rashid,
rrashid@geomar.de

Citation:

Rashid, R., A. Eisenhauer, P. Stocchi, V. Liebetrau, J. Fietzke, A. Rüggeberg, and W.-C. Dullo (2014), Constraining mid to late Holocene relative sea level change in the southern equatorial Pacific Ocean relative to the Society Islands, French Polynesia, *Geochem. Geophys. Geosyst.*, 15, 2601–2615, doi:10.1002/2014GC005272.

Received 29 JAN 2014

Accepted 3 JUN 2014

Accepted article online 6 JUN 2014

Published online 25 JUN 2014

Constraining mid to late Holocene relative sea level change in the southern equatorial Pacific Ocean relative to the Society Islands, French Polynesia

Rashid Rashid¹, Anton Eisenhauer¹, Paolo Stocchi², Volker Liebetrau¹, Jan Fietzke¹, Andres Rüggeberg³, and Wolf-Christian Dullo¹
¹GEOMAR, Helmholtz-Zentrum für Ozeanforschung Kiel, Kiel, Germany, ²NIOZ Royal Netherlands Institute for Sea Research, Texel, Netherlands, ³Department of Geosciences, University of Fribourg, Fribourg, Switzerland

Abstract Precisely quantifying the current climate-related sea level change requires accurate knowledge of long-term geological processes known as Glacial Isostatic Adjustments (GIA). Although the major postglacial melting phase is likely to have ended ~ 6 – 4 ka BP (before present), GIA is still significantly affecting the present-day vertical position of the mean sea surface and the sea bottom. Here we present empirical rsl (relative sea level) data based on U/Th dated fossil corals from reef platforms of the Society Islands, French Polynesia, together with the corresponding GIA-modeling. Fossil coral data constrain the timing and amplitude of rsl variations after the Holocene sea level maximum (HSLM). Upon correction for isostatic island subsidence, we find that local rsl was at least $\sim 1.5 \pm 0.4$ m higher than present at ~ 5.4 ka. Later, minor amplitude variations occurred until ~ 2 ka, when the rsl started dropping to its present position with a rate of ~ 0.4 mm/yr. The data match with predicted rsl curves based on global ice-sheet chronologies confirming the role of GIA-induced ocean siphoning effect throughout the mid to late Holocene. A long lasting Late Holocene highstand superimposed with second-order amplitudinal fluctuations as seen from our data suggest that the theoretical predicted timing of rsl change can still be refined pending future calibration.

1. Introduction

The Intergovernmental Panel on Climate Change (IPCC) predicts a mean sea level rise in the order of ~ 3.5 mm/yr as a consequence of greenhouse warming [Alley *et al.*, 2007]. This is likely to contribute to a sea level rise between 29 and 82 cm by the end of the century [IPCC, 2014]. Since about 10% of human population inhabit low coastal regions and islands [McGranahan *et al.*, 2007], it is fundamental to understand the frequency and amplitude of the several natural and anthropogenic mechanisms which contribute to sea level variations. In particular, the knowledge of present-day and future sea level changes strongly relies on our understanding of the past sea level variations [Houghton, 1996]. Geological data show that during the Quaternary period, glacial and interglacial climate conditions have been characterized by a transfer of $\sim 3\%$ of the global ocean water volume between the continental ice sheets and the oceans [Bard *et al.*, 2010; Blanchon *et al.*, 2009; Eisenhauer *et al.*, 1996; Montaggioni *et al.*, 1996; Montaggioni, 2005; Woodroffe and Horton, 2005]. During the Last Glacial Maximum (LGM; ~ 21 ka) 120–130 m of equivalent sea level were stored in form of large continental ice sheets over North America, Eurasia, Greenland, and Antarctica [Denton and Hughes, 1981]. The post-LGM sea level change was punctuated by short-term periods of slower and faster rise, with higher rates of up to 10–15 m/ka [Bard *et al.*, 1996a; Deschamps *et al.*, 2012; Woodroffe and Horton, 2005] during meltwater pulse 1A (14.6–14.3 ka). Before and after the Younger Dryas event (12.9–11.6 ka) [Carlson, 2010], the rate of sea level rise was at its maximum [Bard *et al.*, 1996a; Fairbanks, 1989; Blanchon *et al.*, 2009] and caused coral reefs to drown [Camoin *et al.*, 2012; Dullo *et al.*, 1998]. Although the trend and rate of global mean sea level (msl) change (commonly known as eustatic sea level change) follows the rate of melting/growth of continental ice masses, several coeval mid to late Holocene sea level indicators based on fossil coral reefs found in different regions show that the timing and amplitude of postglacial sea level variations are not uniform, but strongly depend on the geographical position and varies considerably as a function of the distance from the formerly glaciated areas [Lambeck *et al.*, 2002; Milne *et al.*, 2009; Mitrovica and Peltier, 1991; Mitrovica and Milne, 2002]. Because the msl is an equipotential surface of gravity, it does not only vary in time as a function of addition/removal of ocean water but also spatially according to the

differential variations of the Earth's gravity potential which are triggered by the continental ice-sheet fluctuations [Mitrovica and Peltier, 1991; Peltier, 2002]. Hence, as far as ice-sheets fluctuations are concerned, the oceans do not behave like a bathtub as the eustatic model would imply as it was described in the pioneering study of Suess and Waagen [1888]. When an ice sheet melts, in fact, the lack of gravitational pull which was previously exerted by ice mass on the ocean water results in a sea level drop nearby the formerly glaciated area and in a sea level rise higher than the eustatic value at the opposite end [Mitrovica and Milne, 2002; Woodward, 1888]. Hence, the ocean-averaged sea level change exactly corresponds to the eustatic change [Suess and Waagen, 1888], but the local sea level change may be significantly different, or even opposite in sign. Furthermore, a time-dependent contribution to the msl variation from the ice-sheets fluctuations exists because of the deformability of the solid Earth with respect to ice and ocean surface mass displacements. In fact, during and after the melting of an ice sheet, the formerly glaciated areas undergo isostatic rebound (rise of the land mass) in order reach new isostatic equilibrium. At the same manner, the uplifted area surrounding the formerly glaciated area subsides, as well as the ocean seafloor because of the addition of meltwater [Mitrovica and Milne, 2002]. This implies that the solid Earth response is both immediate and delayed and can be approximated by a Maxwell viscoelastic body. The solid Earth deformations behave like density variations and directly affect the shape of the geoid and the msl, respectively. However, and more importantly, since both the msl and the solid Earth surface deform during and after the melting of an ice sheet, any land based marker (sea level indicator like coral reef corals) would record the msl change with respect to the sea bottom, i.e., the local rsl. The feedbacks described so far drive GIA processes and result in rsl changes which depart from eustasy as a function of the distance from the formerly glaciated areas, of the shape of the ocean basins and of the rheology of the solid Earth.

Geological evidences from South Pacific and Indian Ocean islands show that the last 6.5 ka were characterized by a 1–3 m rsl drop [Banerjee, 2000; Deschamps et al., 2012; Eisenhauer et al., 1993; Grossman et al., 1998; Woodroffe and Horton, 2005] which can be explained by the GIA-induced ocean siphoning effect and the migration of ocean water toward the subsiding peripheral forebulges that surrounded the formerly glaciated areas in the Northern and Southern Hemispheres [Milne and Mitrovica, 1998; Mitrovica and Peltier, 1991; Mitrovica and Milne, 2002]. As a morphological consequence to Mid and Late Holocene regression, the coral reefs from Indian and Pacific Ocean islands developed extended emerged fossil reef platforms which are currently 1–3 m above the msl [Eisenhauer et al., 1999, 1993; Grossman et al., 1998; Montaggioni and Pirazzoli, 1984; Pirazzoli et al., 1988; Woodroffe and Horton, 2005]. Because of the geographical location, the late Holocene sea level regression observed at the Indo-Pacific islands is clearly in contrast with the almost eustatic rsl change recorded at the Caribbean islands [Fairbanks, 1989; Woodroffe and Horton, 2005]. Furthermore, superimposed to the general rsl drop, the Indo-Pacific islands show second-order rsl fluctuations in the range of 0.1–1.0 m [Flood and Frankel, 1989; Pirazzoli et al., 1988; Scoffin and Le Tissier, 1998; Woodroffe et al., 1990; Young et al., 1993] which may be attributed to sea surface temperature (SST) variations in the order of 1–2°C [Goelzer et al., 2012; Levermann et al., 2013].

In general, tropical Pacific areas remain far less understood than their Atlantic counterparts [Camoin and Davies, 1998; Kennedy and Woodroffe, 2002; Montaggioni, 2005]. Also, published rsl records from Indo-Pacific regions and, in particular, from the Society Islands [Montaggioni and Pirazzoli, 1984; Pirazzoli and Montaggioni, 1988; Pirazzoli and Pluet, 1991] are mostly based on radiocarbon dating and consequently carry higher uncertainty due to the lack of information about the ^{14}C residence time [Chappell and Polach, 1991; Eisenhauer et al., 1999; Grossman et al., 1998; Kench et al., 2009; Pirazzoli et al., 1988; Scoffin and Le Tissier, 1998; Woodroffe and McLean, 1990]. Furthermore, the geographical position provided in earlier studies as well as the corresponding elevation above mean sea level are less constrained due to the lack of modern "Global Positioning System (GPS)" and improved tidal and atmospheric pressure corrections.

More robust estimates of mid to late Holocene rsl fluctuations in the Indo-Pacific region can be gained by the comparison of U/Th dated corals from different islands and atolls. In particular, the U/Th dating method is independent of any reservoir ages and provides high precision values ranging from ~2 year old sample up to ~600,000 year old sample [c.f. Stirling and Andersen, 2009]. However, diagenetic changes related to the recrystallization of aragonite to calcite may obscure the actual age of the samples [Bard et al., 1996b; Eisenhauer et al., 1993; Scholz and Mangini, 2007].

The present study aims at better constraining the amplitude and timing of mid to late Holocene rsl changes by means of U/Th dating of fossil corals sampled from emerged platforms of the Society Islands (French

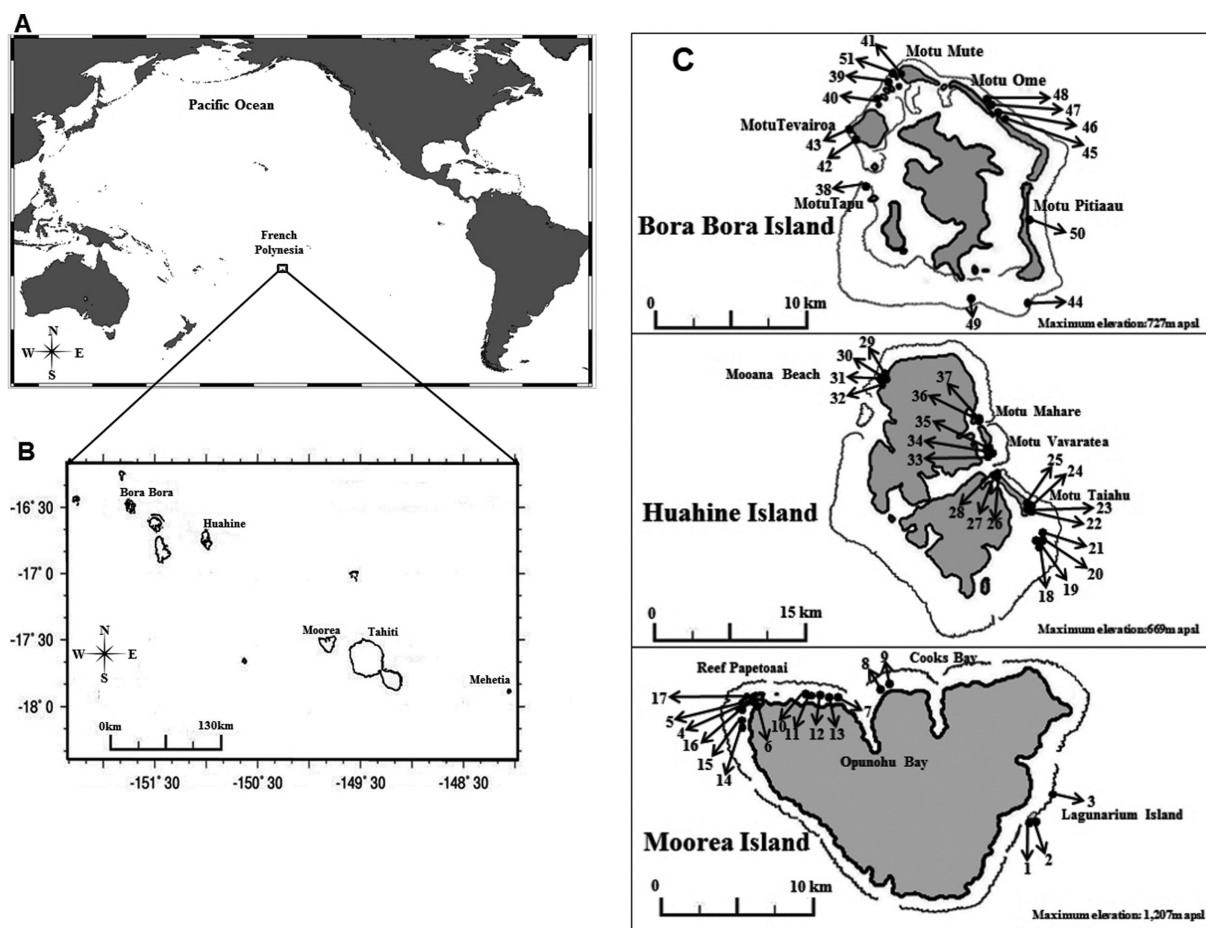


Figure 1. Location of the French Polynesia where (a) Society Islands are located and (b) the islands of Moorea, Huahine, and Bora Bora in particular. (c) The sample sites along the shore lines of Moorea, Huahine, and Bora Bora. Arrows pointing toward numbers refer to Tables 1 and 2.

Polynesia, South Pacific Ocean). The rsl record presented here is compared to theoretical predictions of GIA-induced rsl changes computed for two available global ice-sheet chronologies [Lambeck *et al.*, 1998; Peltier, 2004] by solving the gravitationally self-consistent Sea Level Equation formalism (SLE) [Farrell and Clark, 1976; Mitrovica and Peltier, 1991; Spada and Stocchi, 2007]. Any difference between empirically determined sea level records and theoretical predictions will help to constrain the geophysical models and basic parameters as well as to determine the timing of the postglacial melting of the three major ice reservoirs in North America, Europe, and Antarctica.

2. Samples and Methods

2.1. Sample Location

Samples for this study were collected from Society Islands, French Polynesia (Figures 1a and 1b) because these islands are characterized by extended Holocene emerged fossil reef platforms [Davies and Marshall, 1980; Montaggioni and Pirazzoli, 1984; Pirazzoli and Montaggioni, 1986] being a direct consequence of the decline of the Late Holocene sea level highstand after ~6.5 ka BP. According to the model for epicontinental reef growth [Davies and Marshall, 1980], the presence of these platforms provide suitable sampling localities for mid to late Holocene sea level variations studies [Eisenhauer *et al.*, 1993; Montaggioni and Pirazzoli, 1984; Pirazzoli *et al.*, 1988; Pirazzoli and Montaggioni, 1986; Yu *et al.*, 2010]. The Society archipelago comprises more than 10 islands and atolls elongated in 17°52'S 149°50'W and 15°48'S 154°50'W direction which spread across 720 km of the Pacific Ocean [Duncan and McDougall, 1976; Montaggioni, 2011; Peltier, 2002; Pirazzoli and Montaggioni, 1988]. The islands are elongated in the direction which is virtually parallel to the present absolute motion of the Pacific plate [Blais *et al.*, 2002; Gripp and Gordon, 1990; Uto *et al.*,

Table 1a. Information of Sampling Locations on Moorea^a

Map Code	Sampling Location	Coordinates		Height apsl (m)	Island	Comments
Lagunarium Island						
1	L1–2	17°33′ 7.62″S	149°46′33.46″W	0.75 ± 0.40	Moorea	In situ
2	LI-4	17°33′ 7.62″S	149°46′33.46″W	0.75 ± 0.40	Moorea	In situ
White Light House						
3	WL1	17°32′ 31.00″S	149°45′54.69″W	0.75 ± 0.40	Moorea	In situ
Reef Papetoaai						
4	CB10	17°29′ 27.4″S	149°55′15.4″W	1.80 ± 0.40	Moorea	Conglomerate
5	CB11	17°29′ 18.8″S	149°54′52.6″W	1.80 ± 0.40	Moorea	Conglomerate
6	CB12	17°29′ 29.07″S	149°54′32.9″W	1.80 ± 0.40	Moorea	Conglomerate
7	CB5	17°29′ 08.9″S	149°54′07.6″W	1.80 ± 0.40	Moorea	Displaced
8	RP2	17°29′ 12.59″S	149°53′7.57″W	0.00 ± 0.40	Moorea	In situ
9	RP4	17°29′ 12.59″S	149°53′7.57″W	−0.80 ± 0.40	Moorea	In situ
10	MCM1	17°29′ 7.62″S	149°54′9.74″W	1.10 ± 0.40	Moorea	In situ
11	MCM2	17°29′ 7.62″S	149°54′9.74″W	1.10 ± 0.40	Moorea	In situ
12	MCM5	17°29′ 7.62″S	149°54′9.74″W	1.10 ± 0.40	Moorea	In situ
13	MCM10	17°29′ 8.86″S	149°54′7.64″W	1.10 ± 0.40	Moorea	In situ
14	CM1	17°29′ 34.89″S	149°55′19.98″W	0.75 ± 0.40	Moorea	In situ
15	CM2	17°29′ 34.89″S	149°55′19.98″W	0.75 ± 0.40	Moorea	In situ
16	CM4	17°29′ 26.29″S	149°55′14.83″W	0.75 ± 0.40	Moorea	In situ
17	CM7	17°29′ 18.84″S	149°54′52.60″W	0.75 ± 0.40	Moorea	In situ

^aThe numbers shown in this table indicate the sampling points shown on the map.

2007]. These islands are thought to have originated from a volcanic hot spot presently located around the island of Mehetia about 110 km east of Tahiti [Binard et al., 1991; Binard et al., 1993; Blais et al., 2002; Devey et al., 1990; Nolasco et al., 1998].

According to published chronological studies, the ages of the islands increase with the distance from a hot spot ranging in age from Mehetia (less than 1 Ma old), to Tahiti (~1.67–0.25 Ma old), to Moorea (~2.15–1.36 Ma old), to Huahine (~3.08–2.06 Ma old), to Tahaa (~3.39–1.10 Ma old), to Raiatea (~2.75–2.29 Ma old), and to Maupiti ~5 Ma old [Duncan et al., 1994; Guillou et al., 2005; Uto et al., 2007; White and Duncan, 1996]. The studies have also shown that, as volcanic islands move away from the hot spot, the oceanic crust becomes progressively cooler and denser and gradually subsiding from the level of its formation. In this case, these Society Islands slowly subside as they move further from its point of origin [Neall and Trewick, 2008]. The Holocene subsidence rate of Society Islands has been determined to be ~0 to a maximum of ~0.5 mm/yr [Bard et al., 1996a; Fadil et al., 2011; Lepofsky et al., 1996; Pirazzoli et al., 1985; Pirazzoli and Montaggioni, 1988].

The climate of the Society Islands is tropical with two main seasons. The warm and rainy season (austral summer) runs from November to April. During this period, the conditions are hot and rainy, with the average SST in the order of ~28°C whereas the heavy rains are mostly experienced during December and January. These are the most intense rains along the coastline exposed to the trade winds that usually blow from East (South-East) and North-East direction. During May to October (austral winter), the climate is relatively less humid, with a SST in the order of ~25°C. The available information indicates the tidal range is between 0.3 and 0.4 m [Bongers and Wyrski, 1987; Taylor, 1979; Yates et al., 2013]. This is in general accord with the NOAA tide book indicating an average of 0.5 m for the Society Islands [NOAA, 2013; Seard et al., 2011].

2.2. Sample Collection and Preparation

The samples were collected during April to May 2009 during the CHECKREEF expedition to the Holocene emerged reef platforms at Moorea, Huahine, and Bora Bora (Table 1a, b and c). The main targets for sampling have been in situ *Porites* in general and *Porites* microatolls in specific. Criteria for in situ sampling have been that fossils corals were found upright in growth position and not showing any indications for later displacement. Samples considered being reworked and transported (conglomerates) in Tables 1 and 2 are not considered for the rsl curve. The position of the corals above the present mean sea level (apmsl) was determined by triangulation of the coral's position to the current position of the mean sea level. To achieve this, the laser was placed on top of the sample with the beam pointing horizontally toward the water table. Using a meter rule, the measurement of the elevation was determined relative to the laser beam and the water level. This process was repeated up to 15 times where by the local time is recorded. Using tide table

Table 1b. Information of Sampling Locations on Huahine^a

Map Code	Sampling Location	Coordinates		Height apsl (m)	Island	Comments
Motu Taiahu						
18	H-Tai-1	16°47' 0.50″S	150°56'54.26″W	0.50 ± 0.40	Huahine	In situ
19	H-Tai-2	16°47' 0.50″S	150°56'54.26″W	0.50 ± 0.40	Huahine	In situ
20	H-Tai-3	16°47' 0.50″S	150°56'54.26″W	−0.80 ± 0.40	Huahine	In situ
21	H-Tai-5	16°47' 0.50″S	150°56'54.26″W	1.00 ± 0.40	Huahine	In situ
22	H-Tai-7	16°46' 31.94″S	150°56'54.89″W	−0.25 ± 0.40	Huahine	In situ
23	H-Tai-8	16°46' 31.94″S	150°56'54.89″W	0.30 ± 0.40	Huahine	In situ
24	H-Tai-9	16°46' 31.94″S	150°56'54.89″W	0.00 ± 0.40	Huahine	Microatoll
25	H-Tai-10	16°46' 31.94″S	150°56'54.89″W	0.00 ± 0.40	Huahine	Microatoll
26	H-Tai-11	16°45' 12.13″S	150°57'53.39″W	0.75 ± 0.40	Huahine	In situ
27	H-Tai-12	16°45' 12.13″S	150°57'53.39″W	−0.20 ± 0.40	Huahine	In situ
28	H-Tai-13	16°45' 12.13″S	150°57'53.39″W	−0.20 ± 0.40	Huahine	In situ
Mooana Beach						
29	H-M-1	16°42' 1.51″S	151°2'18.68″W	0.50 ± 0.40	Huahine	In situ
30	H-M-2	16°42' 1.51″S	151°2'18.68″W	0.30 ± 0.40	Huahine	In situ
31	H-M-4	16°42' 1.51″S	151°2'18.68″W	0.10 ± 0.40	Huahine	In situ
32	H-M-5	16°42' 1.51″S	151°2'18.68″W	0.00 ± 0.40	Huahine	In situ
Motu Vavaratea						
33	H-MT-1	16°44' 29.66″S	150°58'16.10″W	1.10 ± 0.40	Huahine	In situ
34	H-MT-2	16°44' 29.66″S	150°58'16.10″W	0.75 ± 0.40	Huahine	in situ
35	H-V-1	16°44' 28.80″S	150°58'15.66″W	0.25 ± 0.40	Huahine	In situ
Pass Tiare (Motu Mahare)						
36	H-PT-1-A	16°43' 14.08″S	150°58'37.37″W	0.00 ± 0.40	Huahine	In situ
37	H-PT-1-2	16°43' 14.08″S	150°58'37.37″W	0.75 ± 0.40	Huahine	In situ

^aThe numbers shown in this table indicate the sampling points shown on the map.

and the local time, the elevation relative to the mean sea level was achieved. These elevations were also compared to our GPS measurement during each time. Certainly, this method is burdened with uncertainties because the sea level position is not well defined due to wave action but careful positioning and repeated measurements allowed the determination of coral positions in the order of ± 0.4 m. Note, concerning the reconstruction of a Late Holocene sea level curve not only the present-day position apmsl rather its past position during corals life time is of certain importance. The past position has to be determined and reconstructed from the individual subsidence rate of the particular island. Local subsidence rates are known (see section 2.4 below) and assumed to be linear. However, the accuracy of the subsidence rate is also burdened with some unknown uncertainty and may also not be linear rather than abrupt and discontinuously. Hence, the uncertainty of about ± 40 cm attributed to our samples may account for the present-day position but also for the uncertainty induced by the subsidence correction. In addition, the height of sea level may also be obscured by the uncertainty of corals position below sea surface. In order to circumvent at least this problem microatolls are of certain interest.

In particular, the elevation of microatolls (sample no. 24, 25, and 45 in Tables 1 and 2) above the sea level put distinct constraints on the position of a past sea level because normally the sea level is only a few centimeters above microatolls surface during their formation [Chappell, 1983; Flora and Ely, 2003; Larcombe et al., 1995; Scoffin et al., 1978; Smithers and Woodroffe, 2001; Woodroffe and McLean, 1990; Woodroffe, 2005]. Selected fossil coral samples were taken out of the platforms using hammers and chisels. The elevation interval from which the samples were taken ranges from -1.5 m to less than ~ 2 m apmsl, respectively. The uncertainty of the sample's elevation determination relative to the present msl was conservatively estimated to be in the order of ± 0.4 m.

Selected samples were cut into slabs (~ 1 cm thick) along the growth direction. Afterward, the slabs were washed with Milli-Q water and dried at room temperature in a clean lab fume hood. Using a diamond saw, samples were further cut into smaller blocks within the parallel growth bands by selecting the best parts visually free from any algal or carbonate infill of the pore volume. These blocks were then cut into small pieces (chips) and transferred into teflon beakers for further cleaning using ultrasonification method [Cheng et al., 2000a]. Cleaned sample were then transferred into a hot plate and dried at $\sim 35^\circ\text{C}$ overnight. Each sample was then crushed into powder and the mineralogy of the samples in terms of aragonite or Mg-calcite was determined by X-Ray diffraction (XRD) method.

Table 1c. Information of Sampling Locations on Bora Bora^a

Map Code	Sampling Location	Coordinates		Height amsl (m)	Island	Comments
<i>Motu Tapu</i>						
38	BB-MP 3/2	16°29' 43.99"S	151°46'46.92"W	1.10 ± 0.40	Bora Bora	In situ
<i>Motu Mute</i>						
39	BB-MP 4/2	16°26' 48.49"S	151°46'3.18"W	1.10 ± 0.40	Bora Bora	In situ
40	BB-MP 2/2	16°27' 22.49"S	151°46'20.20"W	1.10 ± 0.40	Bora Bora	In situ
41	BB-MP 5/3	16°26' 36.14"S	151°45'52.75"W	−1.30 ± 0.40	Bora Bora	in situ
<i>Motu Tevairoa</i>						
42	BB-MP 6/6	16°28' 30.24"S	151°46'55.51"W	−1.30 ± 0.40	Bora Bora	In situ
43	BB-MP 6/5	16°28' 17.90"S	151°47'4.26"W	−1.30 ± 0.40	Bora Bora	In situ
<i>Motu Pitiaau</i>						
44	BB-MX 1/2	16°33' 6.35"S	151°42'20.01"W	1.30 ± 0.40	Bora Bora	In situ
<i>Motu Ome</i>						
45	BB-MX 3/2	16°27' 54.67"S	151°42'44.50"W	0.95 ± 0.40	Bora Bora	Microatoll
46	BB-MX 4/2	16°27' 54.67"S	151°42'44.50"W	1.40 ± 0.40	Bora Bora	In situ
47	BB-MX 5/1	16°27' 50.86"S	151°42'49.35"W	0.95 ± 0.40	Bora Bora	In situ
48	BB-MX 5/3	16°27' 49.99"S	151°42'50.70"W	0.95 ± 0.40	Bora Bora	In situ
<i>Motu Pitiaau</i>						
49	BB-MX 6/3	16°33' 7.49"S	151°44'1.36"W	0.95 ± 0.40	Bora Bora	In situ
50	BB-MX 7/2	16°30' 42.07"S	151°42'4.73"W	1.40 ± 0.40	Bora Bora	In situ
<i>Motu Mute</i>						
51	BB-MM-13	16°26' 36.03"S	151°45'53.24"W	0.65 ± 0.40	Bora Bora	In situ

^aThe numbers shown in this table indicate the sampling points shown on the map.

2.3. Uranium and Thorium Isotope Measurements

Uranium series measurements of coral ages were performed at GEOMAR, Helmholtz Centre for Ocean Research Kiel, Germany. In brief, separation of uranium and thorium from the sample matrix was done using Eichrom-UTEVA resin followed previously published methods [Blanchon *et al.*, 2009; Douville *et al.*, 2010; Fietzke *et al.*, 2005]. Determination of uranium and thorium isotope ratios was done using the multi-ion-counting inductively coupled plasma mass spectroscopy (MC-ICP-MS) approach using the method of Fietzke *et al.* [2005]. The ages were calculated using the half-lives published by Cheng *et al.* [2000b]. For isotope dilution measurements, a combined $^{233}\text{U}/^{236}\text{U}/^{229}\text{Th}$ spike was used with stock solutions calibrated for concentration using NIST-SRM 3164 (U) and NIST-SRM 3159 (Th) as combi-spike, calibrated against CRM-145 uranium standard solution (formerly known as NBL-112A) for uranium isotope composition and against a secular equilibrium standard (HU-1, uranium ore solution) for the precise determination of $^{230}\text{Th}/^{234}\text{U}$ activity ratios. Whole-procedure blank values of this sample set were measured between 0.5 and 1 pg for thorium and between 10 and 20 pg for uranium. Both values are in the range typical of this method and the laboratory [Fietzke *et al.*, 2005].

2.4. Correction for the Subsidence of the Islands

Few studies have been focusing on the assessment of the subsidence rates of the Society Islands [e.g., Fadil *et al.*, 2011; Thomas *et al.*, 2012] mostly on Tahiti Island. For Moorea, Huahine, and Bora Bora, Pirazzoli *et al.* [1985] and Pirazzoli and Montaggioni [1985] conducted a study based on petrological analysis of emerged reef conglomerate available on the shorelines of the islands. The analysis was based on the close inspection of thin sections of exposed coral reef conglomerates. In their study, they have found different layers of the conglomerates corresponding to different diagenetic sequences. The lower sequence exhibit earlier generations of diagenesis developed within marine phreatic zone corresponding to sub tidal environment (e.g., Magnesian Calcite, Pelleted micrite) within interparticle pore spaces. The upper part exhibit the later generation of diagenesis developed in the marine vadose zone corresponding to mid littoral zone (e.g., irregular rims of truncated aragonite fibres and pendant microstalactites) or the splash zone. Using radiocarbon dating, the type of diagenetic imprint and the stratigraphic elevation of the conglomerates specimen, they have been able to calculate the subsidence rates of the Islands. Based on this study, we have directly applied the subsidence rates of Moorea and Huahine (0.14 mm/yr) and Bora Bora (0.05 mm/yr) islands for correction of the elevations of our samples.

3. Results and Discussion

3.1. U/Th-Age Dating

Table 2 summarizes all measured uranium and thorium data and the calculated U/Th ages. For uranium and thorium isotope analysis only samples with no detectable traces of calcite were used for measurements.

Table 2. Uranium/Thorium Isotopic Composition and Ages of Fossil Corals From Moorea, Huahine, and Bora Bora, Society Islands^a

Sample Number	Island	Sample Label	²³⁸ U (ppm)	$\delta^{234}\text{U}(0)$ (‰)	$\delta^{234}\text{U}(T)$ (‰)	²³² Th (ppb)	²³⁰ Th/ ²³⁸ U (dpm/dpm)	²³⁰ Th/ ²³² Th (dpm/dpm)	Age (ka)	Sampling Elevation (m)	Subsidence Corrected Elevation (m)
1	Moorea	**LI-2	2.877 ± 0.004	148 ± 2	150 ± 2	0.0161 ± 0.0001	0.0304 ± 0.0002	16,800 ± 160	2.94 ± 0.03	0.75 ± 0.40	1.16 ± 0.40
2	Moorea	LI-4	3.215 ± 0.004	144 ± 3	145 ± 3	0.0094 ± 0.0001	0.0316 ± 0.0001	33,200 ± 400	3.07 ± 0.02	0.75 ± 0.40	1.18 ± 0.40
3	Moorea	**WL1	2.230 ± 0.003	150 ± 3	151 ± 3	0.0437 ± 0.0003	0.0189 ± 0.0001	3000 ± 30	1.82 ± 0.02	0.75 ± 0.40	1.01 ± 0.40
4	Moorea	CB 10	3.481 ± 0.007	142 ± 4	143 ± 4	0.505 ± 0.011	0.0214 ± 0.0011	400 ± 20	2.06 ± 0.11	1.80 ± 0.40	2.09 ± 0.40
5	Moorea	CB11	2.994 ± 0.005	143 ± 3	144 ± 3	0.0556 ± 0.0002	0.0267 ± 0.0001	4500 ± 20	2.59 ± 0.02	1.80 ± 0.40	2.16 ± 0.40
6	Moorea	*CB12	2.695 ± 0.005	141 ± 3	142 ± 3	0.331 ± 0.003	0.0229 ± 0.0003	600 ± 10	2.22 ± 0.03	1.80 ± 0.40	2.11 ± 0.40
6	Moorea	*CB12 no.2	2.734 ± 0.002	138 ± 3	139 ± 3	0.336 ± 0.004	0.0229 ± 0.0003	600 ± 10	2.22 ± 0.03	1.80 ± 0.40	2.11 ± 0.40
7	Moorea	CB 5	2.433 ± 0.007	143 ± 6	143 ± 6	0.313 ± 0.007	0.00025 ± 0.00002	6 ± 1	0.021 ± 0.002	1.80 ± 0.40	1.80 ± 0.40
8	Moorea	RP2	2.265 ± 0.003	148 ± 3	148 ± 3	0.0225 ± 0.0002	0.00115 ± 0.00003	400 ± 10	0.109 ± 0.003	0.00 ± 0.40	0.02 ± 0.40
9	Moorea	RP4	2.390 ± 0.004	150 ± 3	150 ± 3	0.365 ± 0.003	0.00078 ± 0.00003	20 ± 1	0.072 ± 0.003	-0.80 ± 0.40	-0.79 ± 0.40
10	Moorea	MCM1	3.470 ± 0.011	142 ± 5	143 ± 5	0.093 ± 0.006	0.0311 ± 0.0002	4000 ± 200	3.02 ± 0.04	1.10 ± 0.40	1.52 ± 0.40
11	Moorea	MCM2	2.597 ± 0.005	146 ± 3	147 ± 3	0.910 ± 0.007	0.0271 ± 0.0001	200 ± 2	2.61 ± 0.02	1.10 ± 0.40	1.47 ± 0.40
12	Moorea	MCM5	3.292 ± 0.005	149 ± 4	150 ± 4	0.024 ± 0.006	0.0260 ± 0.0001	10,900 ± 3000	2.51 ± 0.02	1.10 ± 0.40	1.45 ± 0.40
13	Moorea	MCM10	2.684 ± 0.004	149 ± 3	149 ± 3	0.089 ± 0.007	0.0227 ± 0.0002	2100 ± 200	2.19 ± 0.02	1.10 ± 0.40	1.41 ± 0.40
14	Moorea	CM1	3.469 ± 0.005	144 ± 3	146 ± 3	0.0099 ± 0.0001	0.0451 ± 0.0002	48,900 ± 700	4.39 ± 0.04	0.75 ± 0.40	1.37 ± 0.40
15	Moorea	CM2	3.607 ± 0.006	145 ± 3	146 ± 3	0.059 ± 0.0003	0.0407 ± 0.0002	7800 ± 40	3.96 ± 0.03	0.75 ± 0.40	1.31 ± 0.40
16	Moorea	CM4	2.934 ± 0.005	146 ± 3	147 ± 3	0.1583 ± 0.005	0.0378 ± 0.0002	2200 ± 70	3.66 ± 0.03	0.75 ± 0.40	1.26 ± 0.40
17	Moorea	CM7	2.598 ± 0.005	147 ± 3	148 ± 3	0.276 ± 0.007	0.0388 ± 0.0002	1100 ± 20	3.76 ± 0.04	0.75 ± 0.40	1.28 ± 0.40
18	Huahine	H-Tai-1	3.892 ± 0.006	145 ± 2	146 ± 2	0.0045 ± 0.0001	0.0351 ± 0.0001	94,900 ± 1500	3.41 ± 0.02	0.50 ± 0.40	0.98 ± 0.40
18	Huahine	*H-Tai-1 no 2	3.95 ± 0.02	143 ± 2	144 ± 2	0.0045 ± 0.0001	0.0352 ± 0.0003	102,900 ± 78,200	3.41 ± 0.03	0.50 ± 0.40	0.98 ± 0.40
19	Huahine	H-Tai-2	3.367 ± 0.004	144 ± 2	145 ± 2	0.116 ± 0.002	0.0321 ± 0.0003	2900 ± 40	3.12 ± 0.03	0.50 ± 0.40	0.94 ± 0.40
20	Huahine	H-Tai-3	3.532 ± 0.009	142 ± 5	144 ± 5	0.628 ± 0.006	0.0477 ± 0.0002	800 ± 10	4.66 ± 0.05	-0.80 ± 0.40	-0.15 ± 0.40
21	Huahine	H-Tai-5	3.99 ± 0.01	140 ± 5	142 ± 5	0.105 ± 0.007	0.0499 ± 0.0003	5800 ± 400	4.90 ± 0.06	1.00 ± 0.40	1.69 ± 0.40
22	Huahine	*H-Tai-7	3.579 ± 0.008	139 ± 5	141 ± 5	0.098 ± 0.007	0.0495 ± 0.0003	5600 ± 400	4.85 ± 0.06	-0.25 ± 0.40	0.43 ± 0.40
23	Huahine	H-Tai-8	2.656 ± 0.008	142 ± 5	144 ± 5	0.076 ± 0.007	0.0404 ± 0.0003	4400 ± 400	3.94 ± 0.05	0.30 ± 0.40	0.85 ± 0.40
24	Huahine	H-Tai-9	2.964 ± 0.009	142 ± 5	144 ± 5	0.053 ± 0.006	0.0419 ± 0.0012	7200 ± 900	4.08 ± 0.14	0.00 ± 0.40	0.57 ± 0.40
25	Huahine	*H-Tai-10	2.966 ± 0.007	140 ± 5	141 ± 5	0.113 ± 0.008	0.0387 ± 0.0015	3100 ± 200	3.78 ± 0.17	0.00 ± 0.40	0.53 ± 0.40
26	Huahine	H-Tai-11	4.26 ± 0.01	142 ± 4	144 ± 5	0.039 ± 0.006	0.0498 ± 0.0003	16,900 ± 2700	4.88 ± 0.06	0.75 ± 0.40	1.43 ± 0.40
27	Huahine	H-Tai-12	3.44 ± 0.01	149 ± 5	150 ± 5	0.050 ± 0.007	0.0430 ± 0.0004	9100 ± 1300	4.17 ± 0.07	-0.20 ± 0.40	0.38 ± 0.40
28	Huahine	H-Tai-13	2.645 ± 0.007	144 ± 5	146 ± 5	0.020 ± 0.005	0.0403 ± 0.0003	16,800 ± 4500	3.92 ± 0.05	-0.20 ± 0.40	0.35 ± 0.40
29	Huahine	H-M-1	2.596 ± 0.006	144 ± 4	147 ± 2	0.055 ± 0.001	0.0402 ± 0.0002	5900 ± 60	3.92 ± 0.04	0.50 ± 0.40	1.05 ± 0.40
30	Huahine	H-M-2	2.293 ± 0.002	146 ± 2	147 ± 2	0.0109 ± 0.0001	0.0402 ± 0.0001	26,200 ± 300	3.92 ± 0.02	0.30 ± 0.40	0.85 ± 0.40
31	Huahine	HM-4	3.639 ± 0.006	147 ± 3	148 ± 3	0.011 ± 0.004	0.0161 ± 0.0001	15,900 ± 6000	1.55 ± 0.02	0.10 ± 0.40	0.32 ± 0.40
32	Huahine	HM-5	3.183 ± 0.005	147 ± 3	147 ± 3	0.119 ± 0.005	0.0113 ± 0.0001	900 ± 40	1.08 ± 0.02	0.00 ± 0.40	0.15 ± 0.40
33	Huahine	H-MT-1	2.593 ± 0.007	149 ± 5	151 ± 5	0.084 ± 0.001	0.0520 ± 0.0002	5000 ± 30	5.07 ± 0.05	1.10 ± 0.40	1.81 ± 0.40
34	Huahine	*H-MT-2	3.082 ± 0.004	142 ± 2	144 ± 2	0.156 ± 0.001	0.0547 ± 0.0002	3300 ± 20	5.38 ± 0.03	0.75 ± 0.40	1.50 ± 0.40
35	Huahine	H-V-1	2.579 ± 0.003	147 ± 2	147 ± 2	0.0679 ± 0.0003	0.0184 ± 0.0001	2200 ± 10	1.78 ± 0.01	0.25 ± 0.40	0.50 ± 0.40
35	Huahine	H-V-1 no 2	2.736 ± 0.002	147 ± 4	148 ± 4	0.0713 ± 0.0007	0.0187 ± 0.0002	2400 ± 200	1.79 ± 0.02	0.25 ± 0.40	0.50 ± 0.40
36	Huahine	H-PT-1-A	2.807 ± 0.004	144 ± 3	145 ± 3	0.490 ± 0.002	0.0205 ± 0.0002	400 ± 3	1.98 ± 0.02	0.00 ± 0.40	0.28 ± 0.40
37	Huahine	H-PT-1-2	3.937 ± 0.005	142 ± 3	144 ± 3	0.215 ± 0.001	0.0505 ± 0.0002	2900 ± 10	4.95 ± 0.02	0.75 ± 0.40	1.44 ± 0.40
38	Bora Bora	BB-MP 3/2	2.047 ± 0.001	146 ± 1	147 ± 1	0.055 ± 0.005	0.0261 ± 0.0003	3000 ± 300	2.52 ± 0.03	1.10 ± 0.40	1.23 ± 0.40
39	Bora Bora	*BB-MP 4/2	3.142 ± 0.002	144 ± 1	145 ± 1	0.730 ± 0.006	0.0301 ± 0.0002	400 ± 4	2.91 ± 0.02	1.10 ± 0.40	1.25 ± 0.40
40	Bora Bora	BB-MP 2/2	3.021 ± 0.001	144 ± 1	146 ± 1	0.201 ± 0.006	0.0324 ± 0.0002	1500 ± 40	3.13 ± 0.02	1.10 ± 0.40	1.26 ± 0.40
41	Bora Bora	BB-MP 5/3	3.326 ± 0.002	145 ± 1	147 ± 1	0.177 ± 0.005	0.0466 ± 0.0002	2700 ± 80	4.53 ± 0.02	-1.30 ± 0.40	-1.07 ± 0.40
42	Bora Bora	BB-MP 6/6	3.090 ± 0.002	144 ± 1	146 ± 1	0.714 ± 0.005	0.0488 ± 0.0002	700 ± 5	4.75 ± 0.02	-1.30 ± 0.40	-1.06 ± 0.40
43	Bora Bora	*BB-MP 6/5	3.094 ± 0.002	142 ± 1	144 ± 1	0.147 ± 0.007	0.0488 ± 0.0002	3200 ± 150	4.76 ± 0.03	-1.30 ± 0.40	-1.06 ± 0.40
44	Bora Bora	*BB-MX 1/2	3.505 ± 0.002	144 ± 1	145 ± 1	0.107 ± 0.007	0.0313 ± 0.0002	3200 ± 200	3.03 ± 0.02	1.30 ± 0.40	1.45 ± 0.40
45	Bora Bora	BB-MX 3/2	2.767 ± 0.001	145 ± 1	146 ± 1	0.140 ± 0.006	0.0287 ± 0.0002	2000 ± 70	2.77 ± 0.02	0.95 ± 0.40	1.09 ± 0.40
46	Bora Bora	BB-MX 4/2	2.858 ± 0.001	145 ± 1	146 ± 1	0.058 ± 0.005	0.0341 ± 0.0002	5200 ± 400	3.29 ± 0.02	1.40 ± 0.40	1.56 ± 0.40
47	Bora Bora	BB-MX 5/1	2.493 ± 0.001	145 ± 1	146 ± 1	0.021 ± 0.004	0.033 ± 0.0002	12,300 ± 2600	3.18 ± 0.02	0.95 ± 0.40	1.11 ± 0.40
48	Bora Bora	**BB-MX 5/3	2.160 ± 0.001	148 ± 1	149 ± 1	0.055 ± 0.006	0.0312 ± 0.0003	3800 ± 400	3.01 ± 0.03	0.95 ± 0.40	1.10 ± 0.40
49	Bora Bora	*BB-MX 6/3	2.815 ± 0.002	142 ± 1	144 ± 1	0.033 ± 0.006	0.0328 ± 0.0002	8600 ± 1700	3.18 ± 0.03	0.95 ± 0.40	1.11 ± 0.40
50	Bora Bora	*BB-MX 7/2	2.055 ± 0.001	144 ± 1	145 ± 1	0.102 ± 0.007	0.0186 ± 0.0003	1200 ± 70	1.79 ± 0.03	1.40 ± 0.40	1.49 ± 0.40
51	Bora Bora	*BB-MM-13	2.661 ± 0.005	142 ± 3	143 ± 3	0.0049 ± 0.0001	0.0249 ± 0.0001	41,900 ± 700	2.42 ± 0.02	0.65 ± 0.40	0.77 ± 0.40

^aThe $\delta^{234}\text{U}(0)$ indicates the measured $^{234}\text{U}/^{238}\text{U}$ ratios from our samples and the $\delta^{234}\text{U}(T)$ represents the decay corrected activity ratio calculated from the measured $^{234}\text{U}(0)$. All statistical errors are two standard deviations of the mean (2σ mean). * indicates the samples with $\delta^{234}\text{U}(T)$ slightly lower, and ** indicates the values slightly higher than $\delta^{234}\text{U}$ seawater value of $146.8 \pm 0.1\text{‰}$ [Andersen et al., 2010]. For the correction of subsidence of the Islands, we have used 0.14 mm/yr for Moorea and Huahine according to Pirazzoli et al. [1985]. For Bora Bora Island, we have used 0.05 mm/yr [Pirazzoli and Montaggioni, 1985]. All samples have been corrected for initial ^{230}Th by using a $^{230}\text{Th}/^{232}\text{Th}$ activity ratio of 0.6 ± 0.2 [Fietzke et al., 2005].

The data show that ^{238}U concentrations vary between 2.055 ± 0.001 ppm (No. 50, BB-MX7/2) and 4.26 ± 0.01 ppm (No. 26, H-Tai-11) with a mean ^{238}U concentration of 2.986 ± 0.005 ppm. The concentrations of ^{232}Th vary from 0.0045 ± 0.0001 ppb (No. 18, HTai-1) to 0.91 ± 0.01 ppb (No. 11, MCM2) with an

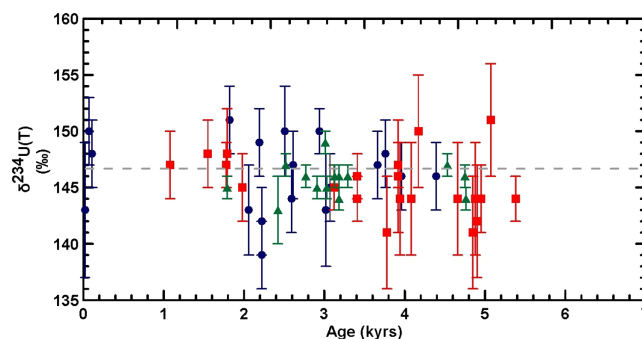


Figure 2. The decay corrected uranium activity ratios, reported as $\delta^{234}\text{U(T)}$ as a function of their corresponding ages. The dashed gray line marks the interval of reported modern sea water uranium isotopic composition $146.8 \pm 0.1\text{‰}$ [Andersen et al., 2010]. Most of our data within uncertainties are plotting within this range. The values below or above this range suggest some marginal open system behavior of these samples [Andersen et al., 2010].

from Figure 2 it is obvious that most of the $\delta^{234}\text{U(T)}$ values fall within their statistical uncertainties in the range of the presently most precise $\delta^{234}\text{U}$ seawater value of $146.8 \pm 0.1\text{‰}$ [Andersen et al., 2010]. Twelve samples (marked with * in the Table 2) are slightly but significantly lower and three samples (marked with **) are significantly higher than this expected value in average by about $3.7 \pm 0.6\text{‰}$. This deviation from the expected value probably suggests a marginal open system behavior of these samples. A difference of 1‰ in the $\delta^{234}\text{U(T)}$ value is expected to change a 4.5 ka old coral in the order of about 5 years. Hence, the average absolute difference of those samples slightly off the accepted value results in an age uncertainty of about ± 20 years. Latter value is within the age uncertainty of our samples being in the order of about 20–30 years and can therefore be considered to be negligible.

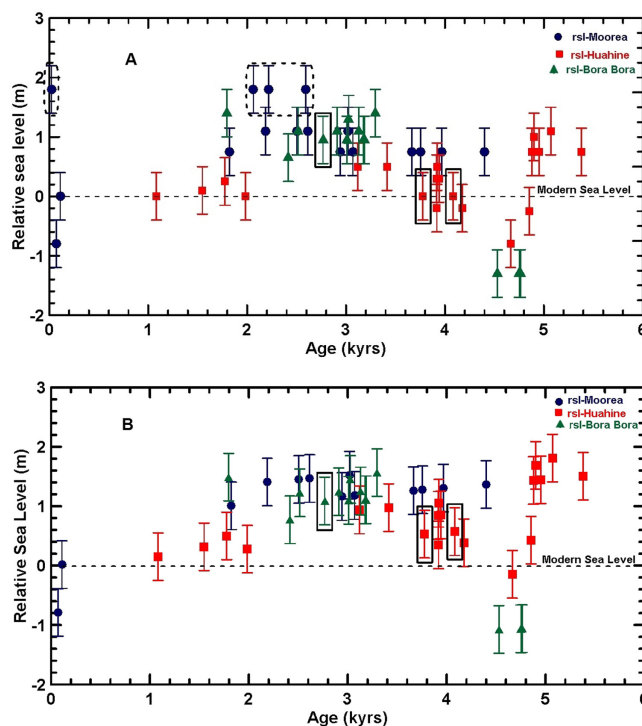


Figure 3. The heights apmsl of the samples are plotted as a function of their corresponding ages. In Figure 3a, dashed circles mark the corals which are either conglomerate or being displaced from their original positions. Samples marked with squares represent microatolls. In Figure 3b, all values have been corrected for their island specific subsidence rate.

average value of 0.163 ± 0.004 ppb. Both the measured ^{232}Th and ^{238}U values are in typical range for young corals from oceanic islands [Chen et al., 1991; Delanghe et al., 2002; Edwards et al., 1988; Yokoyama and Esat, 2004]. The $\delta^{234}\text{U(T)}$ values (Table 2, Figure 2) show lowest values for sample No. 6 of $139 \pm 3\text{‰}$ and highest value of $151 \pm 3\text{‰}$ for sample No. 3 and 33. The $\delta^{234}\text{U(0)}$ values range from $138 \pm 3\text{‰}$ (sample No. 6) to $150 \pm 3\text{‰}$ for sample No. 3 and 9. Taking the $\delta^{234}\text{U}$ isotope value of the sea water into account

4. Society Island Relative Sea level Curve, Subsidence Correction, and Statistical Age Distribution

4.1. In Situ Corals and Microatolls

For establishing an empirical relative sea level curve based on observation only those corals which can be considered to be in situ and being not displaced have to be taken into account. Following this approach we neglect sample Nos. 4, 5, 6 (Tables 1a and 2; marked by dashed circles in Figure 3a) originating from Moorea which were already considered to be conglomerate during the field expedition in 2009. Sample No. 7 (Tables 1a and 2; marked with a dashed circle in Figure 3a) was originally considered to be in situ, however, this sample show an age of ~ 20 years and is

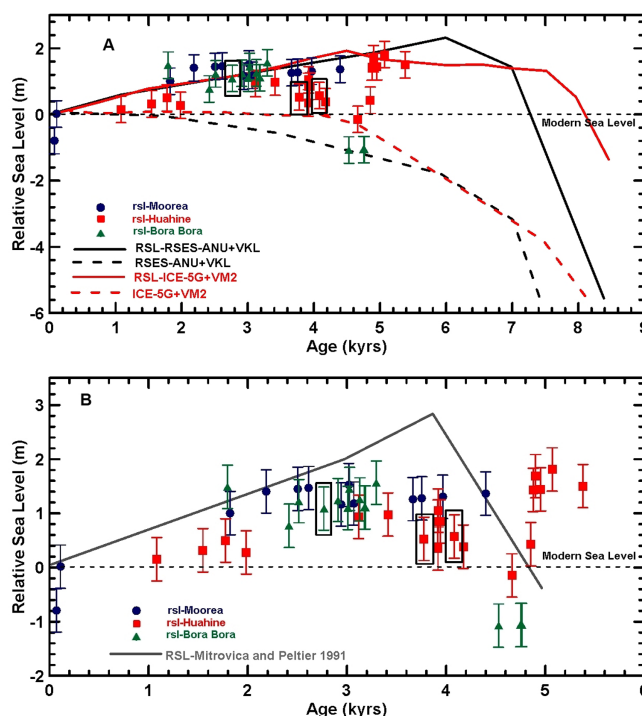


Figure 4. (a) The theoretical predicted rsl curves are compared with empirical observations. The solid black curve represents the predicted rsl according to RSL-RSES-ANU+VKL (ice-sheet model and Mantle profile) and the red solid curve represents the predicted rsl according to RSL-ICE-5G+VM2 (ice-sheet chronology and the viscosity profile). The dashed lines represent the eustatic sea levels. In general, solid curves represent the full result of the sea level equations which incorporates all the solid Earth and gravitational as well as rotational feedback. The dashed curves represent the hypothetical eustatic sea level change for each ice-sheet model. It can be seen that there is a general accord between theoretical predictions and observations. In particular, the microatoll positions are in general accord with the predictions. (b) Our empirical observations are compared with an earlier model ICE-3G ice sheet chronology (grey curve) of Mitrovica and Peltier [1991]. However, there is a general disagreement between the empirical data and this earlier model prediction.

1978; Scott and Rotondo, 1983a, 1983b]. In Figure 3a, it can be seen that the Moorea and Bora Bora corals tend to have the highest elevation whereas the Huahine corals tend to be at the most shallow positions apmsl. Latter observation may reflect differential subsidence rates of the three islands relative to each other as a function of the islands individual cooling which is assumed to be a function of the distance to the former volcanic hot spot. In order to approach the original sea level position during live time of the corals ("paleo-sea level"), the measured elevations of our samples have to be corrected by the subsidence of the studied islands.

For Moorea island which is located ~ 130 km from the hot spot region [Blais et al., 2002], we have applied a subsidence rate of 0.14 mm/yr according to Pirazzoli et al. [1985]. For Bora Bora island which is located ~ 390 km away from the hot spot region the height apmsl is corrected by 0.05 mm/yr only which is the minimum subsidence rate of the Leeward islands in the Society Islands group [Pirazzoli and Montaggioni, 1985]. Although Huahine is located ~ 140 km from Moorea, petrological analysis has claimed that Huahine have similar subsidence rate as Moorea island [Pirazzoli et al., 1985], therefore, the same correction for the subsidence rate was used for this island (Figures 3b, 4a, and 4b). However, after correction, although they overlap within the error, Huahine corals still tend to indicate slightly shallower sea level positions compared to the other two islands. This may indicate that the Huahine subsidence rate is probably slightly higher than the applied rate of 0.14 mm/yr used here for corrections. Note that, our correction and their related uncertainty involves only the uncertainty of our measured sample elevations, because the information about uncertainties concerning the subsidence rates was not available from the cited studies of Pirazzoli and Montaggioni [1985] and Pirazzoli et al. [1985].

actually supposed to be located at the modern msl rather than an elevation of ~ 1.8 m apmsl. Hence, we consider this exceptional sample to be not in situ rather displaced or being a sampling artifact. Therefore, these samples as well as the samples considered to be conglomerate are arbitrarily neglected for further discussion. For later reconstruction of the apparent past sea level, the age and the elevation apmsl of microatolls is of certain interest (marked by squares in Figure 3). Sample No. 24 (H-Tai-9) and No. 25 (H-Tai-10) from Huahine as well as sample 45 (BB-MX 3/2) from Bora Bora represent such microatolls.

4.2. Subsidence Correction

These Society Islands are volcanic in origin and tend to subside as they move away from the asthenospheric bump and as a result of lithospheric cooling with age [McNutt and Menard, 1978]. Therefore, the islands near hot spot tend to subside more rapidly as they move down the slope of the asthenospheric bump compared to the islands which are further away from the hot spot region [McNutt and Menard,

In Figure 3b after subsidence correction the oldest sample data (No. 34, 5.38 ± 0.03 ka) has reached an elevation of $\sim 1.50 \pm 0.40$ m apmsl at Huahine island slightly below the highest coral at a position of 1.81 m apmsl of a coral from Huahine island (No. 33). The microatoll samples No. 24, 25 from Huahine show a subsidence corrected paleo-elevations of 0.57 ± 0.40 m and 0.53 ± 0.40 m apmsl (Figure 3) which is compatible to the paleo-elevation of the microatoll sample 45 from Bora Bora of 1.09 ± 0.40 m apmsl. In particular for the microatoll, the position of the sea level is expected to be within few centimeters of the microatoll position [Smithers and Woodroffe, 2000].

To our knowledge there are only a few measurements by Pirazzoli and Montaggioni [1988] from Bora Bora and Huahine which are directly pertinent to our study. We compare these older ^{14}C -based data with our data presented here after transformation of the ^{14}C ages to U/Th calendar year using the Calib radiocarbon calibration Program (Calib 6.11 program-Marine09) [Stuiver and Reimer, 1993]. Note, that U/Th ages are calendar year ages (2014) whereas ^{14}C ages are stratigraphic ages which have to be converted to calendar year ages by using a well-known ^{14}C -U/Th calibration curve by Stuiver and Reimer [1993]. The converted U/Th ages (in ka BP) for Bora Bora are: (2BB1: 2.97 ± 0.39 (+0.5 m), 2BB7: 3.26 ± 0.36 (+0.4 m), 2BB5: 2.80 ± 0.31 (+0.6 m)) and for Huahine (2HU1: 3.92 ± 0.41 (+0.3 m), 2HU9: 3.55 ± 0.40 (+0.3 m)). For conversion to calendar years reservoir age corrections have been applied between 350 and 400 years according to the geographical locations [Stuiver and Reimer, 1993]. All these earlier measurements are in general accord with our data presented here.

5. Numerical Modeling of the Society Island Sea level Curve(s)

5.1. Geophysical Model

To compute the mid to late Holocene GIA-induced rsl changes at the Society Islands we solve the gravitationally self-consistent Sea Level Equation (SLE) [Farrell and Clark, 1976; Mitrovica and Peltier, 1991] by means of the program SELEN [Spada and Stocchi, 2007]. Solving the SLE for a prescribed continental ice-sheet chronology and solid Earth rheology yields the space and time-dependent rsl change on a global scale [Wu and Peltier, 1983]. The solution of the SLE implies that the gravitational potential of the sea surface is always constant, i.e., that the sea surface corresponds to the equipotential surface of gravity named geoid [Farrell and Clark, 1976; Spada and Stocchi, 2007; Wu and Peltier, 1983]. This implies that ice-sheet thickness variations are compensated by equivalent ocean-averaged sea level variations (eustatic solution), and that the gravity vector is everywhere perpendicular to the sea surface. The two main ingredients of the SLE are (i) the ice-sheet chronology, which describes the ice-sheets thickness variation through time and (ii) the solid Earth rheological model, which describes the response of the solid Earth and of the geoid to ice-sheets thickness variation. We solve the SLE by means of the pseudospectral method, which allows a direct and fast spectral analysis [Milne and Mitrovica, 1998; Mitrovica et al., 1994; Mitrovica and Peltier, 1991]. For this purpose, the solid Earth and geoid deformations are implemented by means of the "Normal Modes Technique" as introduced by Peltier [1974]. The latter assumes a spherically symmetric, self-gravitating, rotating, and radially stratified solid Earth model [Spada et al., 2006] (Spada et al., Modeling sea level changes and geodetic variations by glacial isostasy: The improved SELEN code, submitted, 2012). The latter is a 1-D linear model and does not include lateral heterogeneities. The outer shell is elastic and mimics the lithosphere. Between the lithosphere and the inner inviscid core is the mantle. The latter can be discretized into n Maxwell viscoelastic layers. In this work we discretize the Earth's mantle into two layers, namely the upper mantle and the lower mantle. The lithosphere thickness and the viscosity of the mantle layers are the free parameters.

We employ and compare ICE-5G [Peltier, 2004] and RSES-ANU in global ice-sheets chronologies for the post-LGM deglaciation. The ice-sheets models describe the Late Pleistocene ice-sheets thickness variations until present day and have been constrained by means of geological and archaeological rsl data as well as present-day instrumental observations like GPS-derived vertical and horizontal crustal velocities and Satellite Gravimetry [Peltier, 2004]. Both ice-sheet models depend on the solid Earth rheological, in particular on the thickness of the elastic lithosphere as well as on the number and on the viscosity of Mantle viscoelastic layers which have been employed within the iterative process [Lambeck et al., 1998]. Hence, each ice-sheet model should be employed within the SLE with the accompanying Earth model [Lambeck et al., 1998; Peltier, 2004; Tushingham and Peltier, 1992]. Consequently, we combine ICE-5G chronology with VM2 viscosity profile. The latter is characterized by a 100 km thick elastic lithosphere and by an upper mantle viscosity of 5.0

$\times 10^{20}$ Pa and a lower mantle viscosity of 5.0×10^{21} Pa [Peltier, 2004]. At the same manner we employ RSES-ANU ice-sheets model with a VKL mantle profile. The latter is characterized by a 65 km thick elastic lithosphere and by an upper mantle viscosity of 3.0×10^{20} Pa and a lower mantle viscosity of 10.0×10^{21} Pa [Lambeck et al., 2004]. Hereafter, we refer to the solutions for ICE-5G and VM2 as ICE-5G+VM2, and for RSES-ANU and VKL as RSES-ANU+VKL. We use ETOPO1 model for the initial topography and allow for the self-consistent variation of coastlines as well as for the near-field meltwater damping function [Milne and Mitrovica, 1996, 1998]. Also, we include the rsl variations associated with fluctuations of the Earth's rotation vector [Milne and Mitrovica, 1998].

5.2. Predicted rsl Curves

5.2.1. Eustatic Sea level Change

We compare the rsl curves as predicted for Bora Bora according to RSL-ICE-5G+VM2 (red solid line) and RSL-RSES-ANU+VKL (black solid line), respectively (Figure 4a). The red and black dashed curves represent the eustatic solutions according to ICE-5G and RSES-ANU, respectively. According to ICE-5G (red dashed line), the global mean sea level rises to almost the present position at ~ 4.5 ka although some minor fluctuations occur still later (Figure 4a). A different trend is expected according to RSES-ANU deglaciation, which results in a monotonous sea level rise until present (black dashed line, Figure 4a). For the period under consideration, the main difference between the two eustatic curves depends on the different deglaciation of the Antarctic ice-sheet component in the two global ice-sheets chronologies. While the melting of the Antarctic ice-sheet ends at 4.5 ka in ICE-5G, in RSES-ANU it continues until present day.

5.2.2. Predicted RSL at Society Islands

Both ice-sheets models result in a ~ 2.0 m rsl highstand which is then followed by a drop until present mainly driven by the ocean siphoning effect. In particular, RSL-RSES-ANU+VKL (black solid line in Figure 4a) results in a more peaked highstand at ~ 6 ka, which is then followed by an almost linear rsl drop. The latter is almost specular to the eustatic curve, implying that the local GIA response is significantly stronger than the rate of meltwater release. The RSL-ICE-5G+VM2 model (red solid line) instead, results in an almost stable highstand from about 7.5 ka until 5.0 ka, which is then followed by a short-term rise peaking up at 4.5 ka, when most of the melting ceases. Despite the differences in ice-sheets models and mantle viscosity profiles, our modeled rsl curves show an almost undistinguishable rsl drop after 4.0 ka as a function of the ocean siphoning effect.

While for RSL-ICE-5G+VM2 the rsl drop starts by the very end of the melting phase (4.5 ka), the regression predicted according to RSL-RSES-ANU+VKL starts earlier when ~ 1.8 m of equivalent sea level are still to be released to the oceans from Antarctica. Our GIA modeling results confirm the strength of the ocean siphoning effect, summed to the increase of ocean area due to ice-sheets waxing and flooding of coastal areas, is large enough to fully cloak the eustatic rise.

6. Comparison Between Theoretical Data and Empirical Observations

6.1. Factors Influencing Sea Level Height Observations

In general, *Porites* corals grow from very close to sea level to ~ 25 m below sea level [Cabioch et al., 1999; Carpenter et al., 2008; Pratchett et al., 2013]. Therefore, fossil coral reef cores do not necessarily provide precise constraints on the position of local sea level because of their considerable range of vertical growth. From these arguments, it is clear that we cannot unambiguously establish the actual local sea level curve from sea level observations derived from corals alone. However, we can infer that the Late Holocene sea level curve must have reached a significant height above the present sea level position at this locality and that the true sea level must lie above the corals position. Microatolls are the exception because microatolls are formed at the actual sea level position and may even fall dry during low tides. Following this approach, we infer that any theoretical predicted sea level curve as modeled in the frame of this project must lie at certain distance above the dated corals but with an almost zero distance for a microatoll.

The comparison of our data with our numerical modeling predictions (Figure 4a) shows in general good agreement. In particular, the microatoll sample No. 45 from Bora Bora lies directly along both predicted rsl curves, while Huahine microatolls Nos. 24 and 25 are situated 0.3 m below the theoretical curve.

The scatter in the sea level amplitude as seen from our data may therefore be a function of the differences in the coral's position relative to the sea surface and the differences in the subsidence rate. Considering the

microatolls in our study, they seem to best serve as natural and precise recorders of the sea level. For example, in our data, we can clearly see that, after subsidence correction the microatoll No. 45 from Bora Bora Island clearly marks the sea level around 2.77 ± 0.02 ka (Figures 3b, 4a, and 4b). For Huahine Islands, although the microatolls No. 24 and 25 overlap within the uncertainty with the normal Porites (Sample Nos. 15 (3.96 ± 0.03 ka), 16 (3.66 ± 0.03 ka), and 17 (3.76 ± 0.04 ka)) from Moorea but they are plotted slightly lower in elevation (Figures 3b, 4a, and 4b). From the microatoll study of Christmas island, Woodroffe *et al.* [2012] have observed that although microatolls mark the sea level within few centimeters, they still may show significant differences in elevation as a function of their position in the island. This is probably caused by a differential geoid distortion as a function of the local gravitational field varying as a function between different parts of the island or attenuation of tidal amplitude of the samples collected in the lagoonal areas. Our data can neither support nor preclude the presence of tidal attenuation or geoidal gradient in French Polynesia.

6.2. Comparison of Empirical to Modeled Data

The model-based amplitudes are in general accord with the empirical data concerning the maximum amplitude of ~ 2 m and the timing of the rsl at least for the decline of the Holocene sea level from the highstand to the present-day position. Note, from our rsl data we cannot distinguish which of the ice-models (RSL-ICE-5G+VM2 or RSL-RSES-ANU+VKL), fits best the observations. This is because there are no data available older than ~ 5.5 ka necessary for such a specific model verification.

Although most of the samples lie below the predicted rsl curves, a few data mostly from Moorea and Bora Bora lie slightly above the predictions. We may argue the applied subsidence correction of 0.14 mm/yr for the Moorea corals has been over estimated and the smaller rate is more suitable. We may also argue that the GIA model should be improved by changing the solid Earth model parameters taking into account the local distortions of the geoid, i.e., mantle viscosity values, lithospheric thickness, or even the ice-sheets chronology, or that these corals are not in situ and rather have been displaced from their original positions. In contrast, the applied subsidence correction for Huahine which is also pending independent verification is in general agreement with the theoretical predictions and the other empirical data in general.

In Figure 4b, we also compare the empirical data of this study with earlier model predictions of *Mitrovica and Peltier* [1991] who employed ICE-3G ice-sheet chronology. According to ICE-3G, the postglacial rsl reached modern position approximately 2.5 ka later and resulted in a highstand which is ~ 1 m higher than suggested in this study. It can be seen that most of the empirical data fall within the frame provided by the *Mitrovica and Peltier* [1991] curve and are in general accord with our findings. However, none of the microatoll positions (Nos. 24, 25, 45, marked by squares) are on or close to the *Mitrovica and Peltier* [1991] model curve indicating that the rsl amplitude may be overestimated at these points. In addition, all Huahine corals older than about ~ 4.5 ka (Nos. 21, 22, 26, 33, 34, 37) are also plotting outside the predicted rsl-frame being in contrast to our expectations. Our results support the improvements occurred from the earlier ICE-3G [Tushingham and Peltier, 1992] to the more recent ICE-5G ice-sheet model [Peltier, 2004].

7. Conclusions

Collected in situ fossil corals from the Society Islands, French Polynesia clearly indicate that the local Late Holocene sea level there was higher between at least 5.4 ka until the recent past.

Reconstruction of sea level positions based on dated corals is hampered by the relative wide depth range for coral growth in the water, the subsidence rate of the islands where sample are collected and the gravitational geoid deformation of the local sea level height. Both the predicted rsl curves RSL-ICE-5G+VM2 and RSL-RSES-ANU+VKL (Figure 4a) are in general accord with our empirical data concerning sea level amplitude and timing. In particular, the available microatoll age (No. 45) from Bora Bora is in full support of both model curves after the Holocene sea level highstand.

The available empirical data cannot distinguish between ICE-5G+VM2 and the RSES-ANU+VKL ice-sheet model because no age data are available for corals older than 5.5 ka due to island subsidence.

Both empirical data and modeling indicate that Society Island sea level dropped by ~ 2 m since the Holocene maximum at ~ 4.5 ka BP corresponding to a rate of about 0.4 mm/yr. This value has to be considered when sea level rise due to modern global climate change is considered.

Acknowledgments

The program funding was provided by the ESF funded CHECKREEF project (EI272/22-1, DU129/141-1) and also by GEOMAR, Helmholtz-Zentrum für Ozeanforschung, Kiel. The PhD work of Rashid Rashid was financially supported by the Tanzania Ministry of Education and Vocational Training (MoEVT) in collaboration with DAAD (German Academic Exchange Service) fellowship. We gratefully acknowledge Ana Kolevica, Jutta Heinze, Brendan Ledwig, Patrick Reichert, and Jeroen van der Lubbe for their assistance in sample processing and data analysis. We are also grateful to editors and reviewers for improving the quality of the manuscript.

References

- Alley, R., et al. (2007), *Climate Change 2007: The Physical Science Basis*, Agenda 6, 07, Intergov. Panel on Climate, Geneva, Switzerland.
- Andersen, M. B., C. H. Stirling, E.-K. Potter, A. N. Halliday, S. G. Blake, M. T. McCulloch, B. F. Ayling, and M. J. O'Leary (2010), The timing of sea-level high-stands during Marine Isotope Stages 7.5 and 9: Constraints from the uranium-series dating of fossil corals from Henderson Island, *Geochim. Cosmochim. Acta*, **74**, 3598–3620.
- Banerjee, P. (2000), Holocene and Late Pleistocene relative sea level fluctuations along the east coast of India, *Mar. Geol.*, **167**, 243–260.
- Bard, E., B. Hamelin, M. Arnold, L. F. Montaggioni, G. Cabioch, G. Faure, and F. Rougerie (1996a), Deglacial sea-level record from Tahiti corals and the timing of global meltwater discharge, *Nature*, **382**, 241–244.
- Bard, E., C. Jouannic, B. Hamelin, P. Pirazzoli, M. Arnold, G. Faure, and P. Sumosusastro (1996b), Pleistocene sea levels and tectonic uplift based on dating of corals from Sumba Island, Indonesia, *Geophys. Res. Lett.*, **23**, 1473–1476.
- Bard, E., B. Hamelin, and D. Delanghe-Sabatier (2010), Deglacial meltwater pulse 1B and Younger Dryas sea levels revisited with boreholes at Tahiti, *Science*, **327**, 1235–1237.
- Binard, N., R. Hekinian, J. Cheminée, R. Searle, and P. Stoffers (1991), Morphological and structural studies of the Society and Austral hot-spot regions in the South Pacific, *Tectonophysics*, **186**, 293–312.
- Binard, N., R. Maury, G. Guille, J. Talandier, P. Gillot, and J. Cotten (1993), Mehetia Island, South Pacific: Geology and petrology of the emerged part of the Society hot spot, *J. Volcanol. Geotherm. Res.*, **55**, 239–260.
- Blais, S., G. Guille, H. Guillou, C. Chauvel, R. C. Maury, G. Pernet, and J. Cotten (2002), The island of Maupiti: The oldest emergent volcano in the Society hot spot chain (French Polynesia), *Bull. Soc. Géol. Fr.*, **173**, 45–55.
- Blanchon, P., A. Eisenhauer, J. Fietzke, and V. Liebetrau (2009), Rapid sea-level rise and reef back-stepping at the close of the last interglacial highstand, *Nature*, **458**, 881–884.
- Bongers, T., and K. Wyrski (1987), Sea level at Tahiti-A minimum of variability, *J. Phys. Oceanogr.*, **17**, 164–168.
- Cabioch, G., G. Camoin, and L. Montaggioni (1999), Postglacial growth history of a French Polynesian barrier reef tract, Tahiti, central Pacific, *Sedimentology*, **46**, 985–1000.
- Camoin, G. F., and P. J. Davies (Eds.) (1998), *Reefs and Carbonate Platforms in the Pacific and Indian Oceans*, Blackwell Sci., Oxford; Malden, MA, USA.
- Camoin, G. F., C. Seard, P. Deschamps, J. M. Webster, E. Abbey, J. C. Braga, Y. Iryu, N. Durand, E. Bard, and B. Hamelin (2012), Reef response to sea-level and environmental changes during the last deglaciation: Integrated Ocean Drilling Program Expedition 310, Tahiti sea level, *Geology*, **40**, 643–646.
- Carlson, A. E. (2010), What caused the Younger Dryas cold event?, *Geology*, **38**, 383–384.
- Carpenter, K. E., M. Abrar, G. Aeby, R. B. Aronson, S. Banks, A. Bruckner, A. Chiriboga, J. Cortés, J. C. Delbeek, and L. DeVantier (2008), One-third of reef-building corals face elevated extinction risk from climate change and local impacts, *Science*, **321**, 560–563.
- Chappell, J. (1983), Evidence for smoothly falling sea level relative to north Queensland, Australia, during the past 6,000 yr, *Nature*, **302**, 406–408.
- Chappell, J., and H. Polach (1991), Post-glacial sea-level rise from a coral record at Huon Peninsula, Papua New Guinea, *Nature*, **349**, 147–149.
- Chen, J., H. Curran, B. White, and G. Wasserburg (1991), Precise chronology of the last interglacial period: 234U-230Th data from fossil coral reefs in the Bahamas, *Geol. Soc. Am. Bull.*, **103**, 82–97.
- Cheng, H., J. Adkins, R. L. Edwards, and E. A. Boyle (2000a), U-Th dating of deep-sea corals, *Geochim. Cosmochim. Acta*, **64**, 2401–2416.
- Cheng, H., R. Edwards, J. Hoff, C. Gallup, D. Richards, and Y. Asmerom (2000b), The half-lives of uranium-234 and thorium-230, *Chem. Geol.*, **169**, 17–33.
- Davies, P. J., and J. F. Marshall (1980), A model of epicontinental reef growth, *Nature*, **287**, 37–38.
- Delanghe, D., E. Bard, and B. Hamelin (2002), New TIMS constraints on the uranium-238 and uranium-234 in seawaters from the main ocean basins and the Mediterranean Sea, *Mar. Chem.*, **80**, 79–93.
- Denton, G., and T. Hughes (1981), *The Last Great Ice Sheets*, John Wiley, N. Y.
- Deschamps, P., N. Durand, E. Bard, B. Hamelin, G. Camoin, A. L. Thomas, G. M. Henderson, J. Okuno, and Y. Yokoyama (2012), Ice-sheet collapse and sea-level rise at the Bolling warming 14,600 years ago, *Nature*, **483**, 559–564.
- Devey, C. W., F. Albarede, J. L. Cheminée, A. Michard, R. Mühe, and P. Stoffers (1990), Active submarine volcanism on the Society hotspot swell (West Pacific): A geochemical study, *J. Geophys. Res.*, **95**, 5049–5066.
- Douville, E., E. Sallé, N. Frank, M. Eisele, E. Pons-Branchu, and S. Ayrault (2010), Rapid and accurate U-Th dating of ancient carbonates using inductively coupled plasma-quadrupole mass spectrometry, *Chem. Geol.*, **272**, 1–11.
- Dullo, W., G. Camoin, D. Blomeier, M. Colonna, A. Eisenhauer, G. Faure, J. Casanova, and B. Thomassin (1998), Morphology and sediments of the fore-slopes of Mayotte, Comoro Islands: Direct observations from a submersible, in *Reefs and Carbonate Platforms in the Pacific and Indian Oceans*, Spec. Publ. Int. Ass. Sediment, **25**, pp. 217–236.
- Duncan, R. A., and I. McDougall (1976), Linear volcanism in French polynesia, *J. Volcanol. Geotherm. Res.*, **1**, 197–227.
- Duncan, R. A., M. R. Fisk, W. M. White, and R. L. Nielsen (1994), Tahiti: Geochemical evolution of a French Polynesian volcano, *J. Geophys. Res.*, **99**, 24,341–24,357.
- Edwards, R. L., F. Taylor, and G. Wasserburg (1988), Dating earthquakes with high-precision thorium-230 ages of very young corals, *Earth Planet. Sci. Lett.*, **90**, 371–381.
- Eisenhauer, A., G. J. Wasserburg, J. H. Chen, G. Bonani, L. B. Collins, Z. R. Zhu, and K. H. Wyrwoll (1993), Holocene sea-level determination relative to the Australian continent: U/Th (TIMS) and ¹⁴C (AMS) dating of coral cores from the Abrolhos Islands, *Earth Planet. Sci. Lett.*, **114**, 529–547.
- Eisenhauer, A., Z. Zhu, L. Collins, K. Wyrwoll, and R. Eichstatter (1996), The Last Interglacial sea level change: New evidence from the Abrolhos islands, West Australia, *Geol. Rundsch.*, **85**, 606–614.
- Eisenhauer, A., G. Heiss, C. Sheppard, and W. Dullo (1999), Reef and island formation and Late Holocene sea-level changes in the Chagos islands, in *Ecology of the Chagos Archipelago*, pp. 21–31, Linnean Society Occasional Publications, London.
- Fadil, A., L. Sichoix, J. P. Barriot, P. Ortéga, and P. Willis (2011), Evidence for a slow subsidence of the Tahiti Island from GPS, DORIS, and combined satellite, *Comptes Rendus Geosci.*, **343**, 331–341.
- Fairbanks, R. G. (1989), A 17,000-year glacio-eustatic sea level record: Influence of glacial melting rates on the Younger Dryas event and deep-ocean circulation, *Nature*, **342**, 637–642.
- Farrell, W., and J. A. Clark (1976), On postglacial sea level, *Geophys. J. R. Astron. Soc.*, **46**, 647–667.

- Fietzke, J., V. Liebetrau, A. Eisenhauer, and C. Dullo (2005), Determination of uranium isotope ratios by multi-static MIC-ICP-MS: Method and implementation for precise U-and Th-series isotope measurements, *J. Anal. At. Spectrom.*, **20**, 395–401.
- Flood, P., and E. Frankel (1989), Late Holocene higher sea level indicators from eastern Australia, *Mar. Geol.*, **90**, 193–195.
- Flora, C. J., and P. S. Ely (2003), Surface growth rings of *Porites lutea* microatolls accurately track their annual growth, *Northwest Sci.*, **77**, 237–245.
- Goelzer, H., P. Huybrechts, S. Raper, M. Loutre, H. Goosse, and T. Fichefet (2012), Millennial total sea-level commitments projected with the Earth system model of intermediate complexity LOVECLIM, *Environ. Res. Lett.*, **7**, 045401.
- Gripp, A. E., and R. G. Gordon (1990), Current plate velocities relative to the hotspots incorporating the NUVEL-1 global plate motion model, *Geophys. Res. Lett.*, **17**, 1109–1112.
- Grossman, E. E., C. H. Fletcher III, and B. M. Richmond (1998), The Holocene sea-level highstand in the equatorial Pacific: Analysis of the insular paleosea-level database, *Coral Reefs*, **17**, 309–327.
- Guillou, H., R. C. Maury, S. Blais, J. Cotten, C. Legendre, G. Guille, and M. Caroff (2005), Age progression along the Society hotspot chain (French Polynesia) based on new unspiked K-Ar ages, *Bull. Soc. Géol. Fr.*, **176**, 135–150.
- Houghton, J. T. (1996), *Climate Change 1995: The Science of Climate Change: Contribution of Working Group I to the Second Assessment Report of the Intergovernmental Panel on Climate Change*, Cambridge Univ. Press, Cambridge, U. K.
- IPCC (2014), *Climate Change 2013: The Physical Science Basis. Working Group I Contribution to the Fifth Assessment Report of the Intergovernmental Panel on Climate Change*, edited by T. F. Stocker et al., Cambridge Univ. Press, Cambridge, U. K.
- Kench, P., S. Smithers, R. McLean, and S. Nichol (2009), Holocene reef growth in the Maldives: Evidence of a mid-Holocene sea-level highstand in the central Indian Ocean, *Geology*, **37**, 455–458.
- Kennedy, D., and C. Woodroffe (2002), Fringing reef growth and morphology: A review, *Earth Sci. Rev.*, **57**, 255–277.
- Lambeck, K., C. Smithers, and M. Ekman (1998), Tests of glacial rebound models for Fennoscandia based on instrumented sea-and lake-level records, *Geophys. J. Int.*, **135**, 375–387.
- Lambeck, K., Y. Yokoyama, and T. Purcell (2002), Into and out of the Last glacial maximum: Sea-level change during oxygen isotope stages 3 and 2, *Quat. Sci. Rev.*, **21**, 343–360.
- Lambeck, K., F. Antonioli, A. Purcell, and S. Silenzi (2004), Sea-level change along the Italian coast for the past 10,000 yr, *Quat. Sci. Rev.*, **23**, 1567–1598.
- Larcombe, P., R. Carter, J. Dye, M. Gagan, and D. Johnson (1995), New evidence for episodic post-glacial sea-level rise, central Great Barrier Reef, Australia, *Mar. Geol.*, **127**, 1–44.
- Lepofsky, D., P. V. Kirch, and K. P. Lertzman (1996), Stratigraphic and paleobotanical evidence for prehistoric human-induced environmental disturbance on Mo'orea, French Polynesia, *Pac. Sci.*, **50**, 253–273.
- Levermann, A., P. U. Clark, B. Marzeion, G. A. Milne, D. Pollard, V. Radic, and A. Robinson (2013), The multimillennial sea-level commitment of global warming, *Proc. Natl. Acad. Sci. U. S. A.*, **110**, 13,745–13,750.
- McGranahan, G., D. Balk, and B. Anderson (2007), The rising tide: Assessing the risks of climate change and human settlements in low elevation coastal zones, *Environ. Urbanization*, **19**, 17–37.
- McNutt, M., and H. Menard (1978), Lithospheric flexure and uplifted atolls, *J. Geophys. Res.*, **83**, 1206–1212.
- Milne, G. A., and J. X. Mitrovica (1996), Postglacial sea-level change on a rotating earth: First results from a gravitationally self-consistent sea-level equation, *Geophys. J. Int.*, **126**, F13–F20.
- Milne, G. A., and J. X. Mitrovica (1998), Postglacial sea-level change on a rotating earth, *Geophys. J. Int.*, **133**, 1–19.
- Milne, G. A., W. R. Gehrels, C. W. Hughes, and M. E. Tamisiea (2009), Identifying the causes of sea-level change, *Nat. Geosci.*, **2**, 471–478.
- Mitrovica, J., J. Davis, and I. Shapiro (1994), A spectral formalism for computing three-dimensional deformations due to surface loads: 2. Present-day glacial isostatic adjustment, *J. Geophys. Res.*, **99**, 7075–7101.
- Mitrovica, J. X., and G. A. Milne (2002), On the origin of late Holocene sea-level highstands within equatorial ocean basins, *Quat. Sci. Rev.*, **21**, 2179–2190.
- Mitrovica, J. X., and W. Peltier (1991), On postglacial geoid subsidence over the equatorial oceans, *J. Geophys. Res.*, **96**, 20,053–20,071.
- Montaggioni, L. (2011), Tahiti/Society Islands, in *Encyclopedia of Modern Coral Reefs: Structure, Form and Process*, edited by D. Hopley, pp. 1073–1075, Springer, Netherlands.
- Montaggioni, L., G. Cabioch, G. Faure, and F. Rougerie (1996), Deglacial sea-level record from Tahiti corals and the timing of global melt-water discharge, *Nature*, **382**, 18.
- Montaggioni, L. F. (2005), History of Indo-Pacific coral reef systems since the last glaciation: Development patterns and controlling factors, *Earth Sci. Rev.*, **71**, 1–75.
- Montaggioni, L. F., and P. A. Pirazzoli (1984), The significance of exposed coral conglomerates from French Polynesia (Pacific Ocean) as indicators of recent relative sea-level changes, *Coral Reefs*, **3**, 29–42.
- Neall, V. E., and S. A. Trewick (2008), The age and origin of the Pacific islands: A geological overview, *Philos. Trans. R. Soc. B*, **363**, 3293–3308.
- NOAA (2013), *Tide Tables 2013, High and Low Water Predictions Central and Western Pacific Ocean and Indian Ocean*, North Wind Publ., Brewer, Maine.
- Nolasco, R., P. Tarits, J. H. Filloux, and A. D. Chave (1998), Magnetotelluric imaging of the Society Islands hotspot, *J. Geophys. Res.*, **103**, 30,287–30,309.
- Peltier, W. (1974), The impulse response of a Maxwell Earth, *Rev. Geophys.*, **12**, 649–669.
- Peltier, W. (2004), Global glacial isostasy and the surface of the ice-age Earth: The ICE-5G (VM2) model and GRACE, *Annu. Rev. Earth Planet. Sci.*, **32**, 111–149.
- Peltier, W. R. (2002), On eustatic sea level history: Last Glacial Maximum to Holocene, *Quat. Sci. Rev.*, **21**, 377–396.
- Pirazzoli, P., and L. Montaggioni (1985), Lithospheric deformation in French Polynesia (Pacific Ocean) as deduced from Quaternary shorelines, paper presented at Proceedings of the 5th International Coral Reef Congress, Tahiti.
- Pirazzoli, P., L. Montaggioni, G. Delibrias, G. Faure, and B. Salvat (1985), Late Holocene sea-level changes in the Society Islands and in the northwest Tuamotu atolls, paper presented at Proceedings of the 5th International Coral Reef Congress, Tahiti.
- Pirazzoli, P., L. F. Montaggioni, B. Salvat, and G. Faure (1988), Late Holocene sea level indicators from twelve atolls in the central and eastern Tuamotus (Pacific Ocean), *Coral Reefs*, **7**, 57–68.
- Pirazzoli, P. A., and L. F. Montaggioni (1986), Late Holocene sea-level changes in the northwest Tuamotu islands, French Polynesia, *Quat. Res.*, **25**, 350–368.
- Pirazzoli, P. A., and L. F. Montaggioni (1988), Holocene sea-level changes in French Polynesia, *Palaeogeogr. Palaeoclimatol. Palaeoecol.*, **68**, 153–175.

- Pirazzoli, P. A., and J. Pluett (1991), Holocene changes in sea level as climate proxy data in Europe. Evaluation of Climate Proxy Data in Relation to the European Holocene, *Paleoklimaforschung*, **6**, 205–225.
- Pratchett, M. S., D. McCowan, J. A. Maynard, and S. F. Heron (2013), Changes in bleaching susceptibility among corals subject to ocean warming and recurrent bleaching in Moorea, French Polynesia, *PLoS One*, **8**, e70443.
- Scholz, D., and A. Mangini (2007), How precise are U-series coral ages?, *Geochim. Cosmochim. Acta*, **71**, 1935–1948.
- Scoffin, T., and M. Le Tissier (1998), Late Holocene sea level and reef-flat progradation, Phuket, South Thailand, *Coral Reefs*, **17**, 273–276.
- Scoffin, T. P., D. Stoddart, and B. R. Rosen (1978), The nature and significance of microatolls, *Philos. Trans. R. Soc. London B*, **284**, 99–122.
- Scott, G. A., and G. M. Rotondo (1983a), A model for the development of types of atolls and volcanic islands on the Pacific lithospheric plate, *Atoll Res. Bull.*, **260**, 33.
- Scott, G. A., and G. M. Rotondo (1983b), A model to explain the differences between Pacific plate island-atoll types, *Coral Reefs*, **1**, 139–150.
- Seard, C., G. Camoin, Y. Yokoyama, H. Matsuzaki, N. Durand, E. Bard, S. Sepulcre, and P. Deschamps (2011), Microbialite development patterns in the last deglacial reefs from Tahiti (French Polynesia; IODP Expedition# 310): Implications on reef framework architecture, *Mar. Geol.*, **279**, 63–86.
- Smithers, S. G., and C. D. Woodroffe (2000), Microatolls as sea-level indicators on a mid-ocean atoll, *Mar. Geol.*, **168**, 61–78.
- Smithers, S. G., and C. D. Woodroffe (2001), Coral microatolls and 20th century sea level in the eastern Indian Ocean, *Earth Planet. Sci. Lett.*, **191**, 173–184.
- Spada, G., and P. Stocchi (2007), SELEN: A Fortran 90 program for solving the “sea-level equation,” Modeling sea level changes and geodetic variations by glacial isostasy: The improved SELEN code, *Comput. Geosci.*, **33**, 538–562.
- Spada, G., A. Antonioli, S. Cianetti, and C. Giunchi (2006), Glacial isostatic adjustment and relative sea-level changes: The role of lithospheric and upper mantle heterogeneities in a 3-D spherical Earth, *Geophys. J. Int.*, **165**, 692–702.
- Stirling, C. H., and M. B. Andersen (2009), Uranium-series dating of fossil coral reefs: Extending the sea-level record beyond the last glacial cycle, *Earth Planet. Sci. Lett.*, **284**, 269–283.
- Stuiver, M., and P. Reimer (1993), Extended (super 14) C data base and revised CALIB 3.0 (super 14) C age calibration program, *Radiocarbon*, **35**, 215–230.
- Suess, E., and L. Waagen (1888), *Das Antlitz der Erde*, vol. 2, F. Tempsky, Prague and Vienna, G. Freytag, Leipzig, 703 pp.
- Taylor, F. J. (1979), Rhizophora in the Society Islands, *Pac. Sci.*, **33**, 173–176.
- Thomas, A. L., K. Fujita, Y. Iryu, E. Bard, G. Cabioch, G. Camoin, J. E. Cole, P. Deschamps, N. Durand, and B. Hamelin (2012), Assessing subsidence rates and paleo water-depths for Tahiti reefs using U–Th chronology of altered corals, *Mar. Geol.*, **295**, 86–94.
- Tushingham, A. M., and W. Peltier (1992), Validation of the ICE-3G Model of Würm–Wisconsin Deglaciation using a global data base of relative sea level histories, *J. Geophys. Res.*, **97**, 3285–3304.
- Uto, K., Y. Yamamoto, M. Sudo, S. Uchiumi, O. Ishizuka, T. Kogiso, and H. Tsunakawa (2007), New K–Ar ages of the Society Islands, French Polynesia, and implications for the Society hotspot feature, *Earth Planets Space*, **59**, 879–885.
- White, W. M., and R. A. Duncan (1996), Geochemistry and geochronology of the Society Islands: New evidence for deep mantle recycling, *Geophys. Monogr. AGU*, **95**, 183–206.
- Woodroffe, C., and R. McLean (1990), Microatolls and recent sea level change on coral atolls, *Nature*, **344**, 531–534.
- Woodroffe, C., R. McLean, H. Polach, and E. Wallensky (1990), Sea level and coral atolls: Late Holocene emergence in the Indian Ocean, *Geology*, **18**, 62–66.
- Woodroffe, C. D. (2005), Late Quaternary sea-level highstands in the central and eastern Indian Ocean: A review, *Global Planet. Change*, **49**, 121–138.
- Woodroffe, C. D., H. V. McGregor, K. Lambeck, S. G. Smithers, and D. Fink (2012), Mid-Pacific microatolls record sea-level stability over the past 5000 yr, *Geology*, **40**, 951–954.
- Woodroffe, S. A., and B. P. Horton (2005), Holocene sea-level changes in the Indo-Pacific, *J. Asian Earth Sci.*, **25**, 29–43.
- Woodward, R. S. (1888), On the form and position of the sea level, *U.S. Geol. Surv. Bull.*, **48**, 87–170.
- Wu, P., and W. Peltier (1983), Glacial isostatic adjustment and the free air gravity anomaly as a constraint on deep mantle viscosity, *Geophys. J. R. Astron. Soc.*, **74**, 377–449.
- Yates, M., G. Le Cozannet, M. Garcin, E. Salaï, and P. Walker (2013), Multidecadal atoll shoreline change on Manihi and Manuae, French Polynesia, *J. Coastal Res.*, **29**, 870–882.
- Yokoyama, Y., and T. Esat (2004), Long term variations of uranium isotopes and radiocarbon in the surface seawater recorded in corals, *Global Environ. Change Ocean Land*, **1**, 279–309.
- Young, R., E. Bryant, D. Price, L. Wirth, and M. Pease (1993), Theoretical constraints and chronological evidence of Holocene coastal development in central and southern New South Wales, Australia, *Geomorphology*, **7**, 317–329.
- Yu, K. F., J. X. Zhao, M. G. Lawrence, and Y. Feng (2010), Timing and duration of growth hiatuses in mid Holocene massive Porites corals from the northern South China Sea, *J. Quat. Sci.*, **25**, 1284–1292.